DOI: 10.1002/cssc.200800188

Ethanol Oxidation on Electrocatalysts Obtained by Spontaneous Deposition of Palladium onto Nickel-Zinc Materials

Valentina Bambagioni,[a] Claudio Bianchini,*[a] Jonathan Filippi,[a] Werner Oberhauser,[a] Andrea Marchionni,[a] Francesco Vizza,*[a] Rinaldo Psaro,[b] Laura Sordelli,[b] Maria Luisa Foresti,[c] and Massimo Innocenti[c]

Ni-Zn and Ni-Zn-P alloys supported on Vulcan XC-72 are effective materials for the spontaneous deposition of palladium through redox transmetalation with Pd^{IV} salts. The materials obtained, Pd-(Ni-Zn)/C and Pd-(Ni-Zn-P)/C, have been characterized by a variety of techniques. The analytical and spectroscopic data show that the surface of Pd-(Ni-Zn)/C and Pd-(Ni-Zn-P)/C contain very small, highly dispersed, and highly crystalline palladium clusters as well as single palladium sites, likely stabilized by interaction with oxygen atoms from Ni–O moieties. As a reference material, a nanostructured Pd/C material was prepared by reduction of an aqueous solution of $PdCl_2$/HCl with ethylene glycol in the presence of Vulcan XC-72. In Pd/C, the Pd particles are larger, less dispersed, and much less crystalline. Glassy carbon electrodes coated with the Pd-(Ni-Zn)/C and Pd-(Ni-Zn-P)/C materials, containing very low Pd loadings (22–25 $\mu g\,cm^{-2}$), were studied for the oxidation of ethanol in alkaline media in half cells and provided excellent results in terms of both specific current (as high as 3600 $A\,g(Pd)^{-1}$ at room temperature) and onset potential (as low as −0.6 V vs Ag/AgCl/KCl_{sat}).

Introduction

Primary alcohols with a molecular weight higher than that of methanol are arousing major interest as fuels in direct alcohol fuel cells (DAFC) for various reasons, including their low toxicity, high boiling point, high specific energy and, most importantly, the capacity of some of them to be renewable.[1–4] Included in this group is ethanol, which can be produced on a massive scale from biomass feedstocks originating from agriculture (first-generation bioethanol), forestry and urban residues (second-generation bioethanol). Also, ethanol has a specific energy (6 $kWh\,kg^{-1}$) comparable to that of gasoline (10–11 $kWh\,kg^{-1}$).

Despite the high cost, platinum is still the most commonly used metal in manufacturing anode catalysts for fuel-cell electrodes.[5] However, apart from methanol for which there exists platinum-based catalysts capable of producing power densities of several tens of $mW\,cm^{-2}$, the higher alcohols such as ethanol are difficult to oxidize on platinum or platinum alloyed with either noble or non-noble metals.[1–4] In particular, no known anode catalyst based on platinum, even at high metal loadings, has demonstrated the capacity to produce acceptable power densities in a direct ethanol fuel cell (DEFC). The best performances so far reported were obtained in active cells at temperatures above 90 °C with binary Pt-Sn and Pt-Ru anode catalysts in conjunction with platinum-based cathodes and Nafion proton-exchange membranes.[1–4] However, the power densities never exceed 60–70 $mW\,cm^{-2}$ and the overall efficiency suffers the consequences of the partial oxidation of ethanol to mixtures of acetaldehyde, acetic acid and CO_2.[1–4] It has been established that a major contribution to the overpotentials of Pt-based anodes in DEFCs is provided by the poisoning of catalysts by CO, which is an intermediate of ethanol oxidation.[1,2,6]

For all of these reasons, notable efforts are being carried out in the design of new catalytic structures for DEFC anodes that either do not contain platinum or contain tiny amounts of this metal and, most of all, are able to oxidize ethanol with fast kinetics, tolerable deactivation with time and high substrate concentration.

Palladium has recently aroused notable interest in electrocatalysis as it is more abundant in nature, hence less expensive than platinum and has the capacity to promote the oxidation of several alcohols, including ethanol, in alkaline media.[2–4] Current synthetic methods for the preparation of Pd-based electrocatalysts for anodes of DAFCs are manifold.[7] Electroless procedures generally involve the adsorption of a palladium

[a] *Dr. V. Bambagioni, Dr. C. Bianchini, Dr. J. Filippi, Dr. W. Oberhauser, Dr. A. Marchionni, Dr. F. Vizza*
Istituto di Chimica dei Composti Organometallici (ICCOM-CNR)
via Madonna del Piano 10, 50019 Sesto Fiorentino (Italy)
Fax: (+39) 0555225203
E-mail: claudio.bianchini@iccom.cnr.it

[b] *Dr. R. Psaro, Dr. L. Sordelli*
Istituto di Scienze e Tecnologie Molecolari (ISTM-CNR)
via C. Golgi 19, 20133 Milano (Italy)

[c] *Dr. M. L. Foresti, M. Innocenti*
Dipartimento di Chimica, Università degli Studi di Firenze
via della Lastruccia 3, 50019 Sesto Fiorentino (Italy)

Supporting information for this article is available on the WWW under http://dx.doi.org/10.1002/cssc.200800188.

compound ($PdCl_2$, K_2PdCl_4 or H_2PdCl_4), alone or in conjunction with a salt of another metal, onto a conductive support material, followed by reduction in aqueous dispersion with an appropriate reducing agent that may also act as templating agent to favor the formation of nanosized metal particles ($NaBH_4$, ethylene glycol, hydrazine, tannic acid, formic acid, formaldehyde, hydrogen gas).[8–10] Alternatively, surfactant-stabilized colloidal Pd can be independently prepared and later mixed with a carbon black.[11] A large variety of conductive materials have been used to support Pd nanoparticles, including carbon blacks like Vulcan XC-72, alone[8] or in combination with either nanocrystalline metal oxides (NiO, CeO_2, Co_3O_4, Mn_3O_4)[12,13] or tungsten carbide nanocrystals,[14] carbon microspheres,[15] coin-like hollow carbons,[16] ultrahigh-surface hollow carbon spheres,[17] carbonized porous anodic alumina,[18] carbonized TiO_2 nanotubes,[19] multiwalled carbon nanotubes[20] and activated carbon nanofibers.[20]

Electrochemical methods for the preparation of anode electrocatalysts for DAFCs involve the electrodeposition of one metal at a time, eventually followed by the electrodeposition of other metals. Highly ordered Pd nanowires arrays have been prepared by template-electrodeposition on glassy carbon electrodes,[21] while cyclic potential sweep techniques have been used to prepare Pd thin films on polycrystalline Pt or Au substrates.[22]

As an alternative to electroless and electrodeposition techniques for manufacturing electroactive materials, increasing attention has been recently paid to the spontaneous deposition of noble metals onto less-noble metal particles or metal surfaces.[23–32] Spontaneous deposition is currently emerging as a viable technique for creating new catalyst architectures as well as allowing single noble-metal sites to be introduced over the surface of a non-noble-metal phase. Some applications of the spontaneous deposition technique to the preparation of anode electrocatalysts for fuel cells have been reported,[25–27,32] including only one example of an active Pt-Ru anode catalyst in a DEFC.[25]

The mechanism of the spontaneous deposition is still not well understood, and this concept is often confused with the electroless deposition technique.[33] Perhaps the best definition has been provided by Cheon and co-workers,[24] who stated: "*When a metal-ligand complex in a positive metal oxidation state ($M_{II}^{n+}L_i^{n-}$) approaches another metal surface (M_I), $M_{II}L_i$ molecules can be reduced through the sacrificial oxidation of the M_I surface atoms to produce M_{II} deposition on the M_I metal surface via a redox trasmetalation process*".

A scheme representing the spontaneous deposition of a high-valent metal through redox transmetalation is shown in Scheme 1 for a hypothetical metal phase supported on a conductive material.

A non-ambiguous example of spontaneous deposition, leading to the formation of a Pt-Ni alloy, was achieved by Nakashima et al. by treatment of nickel discs with an aqueous solution of H_2PtCl_6 under acidic conditions.[34] The redox reaction that would occur [Eq. (1)] generates a modified nickel electrode that is active in the catalytic oxidation of methanol.

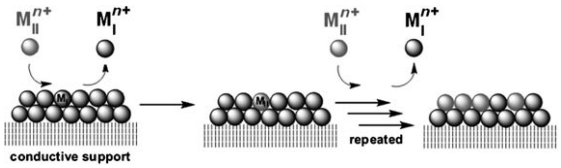

Scheme 1. Deposition of metal M_{II} onto particles of metal M_I by redox transmetalation.

$$Pt^{II} + Ni^0 \rightarrow Pt^0 + Ni^{II} \quad (1)$$

While there are clear cases of the correctness of the definition provided by Cheon and co-workers,[24] there are also examples on the borderline between spontaneous and electroless deposition. This might be the case of the depositions of Pt on either a Ru(001) single surface[31] or Ru nanoparticles supported on Vulcan XC-72R.[25] Indeed, Adzic and co-workers have argued that the oxidative dissolution of Ru by action of $[PtCl_6]^{2-}$ can be excluded because it would occur at a potential more positive than the equilibrium potential of $Pt/[PtCl_6]^{2-}$.[31] As a thermodynamically viable mechanistic alternative, Adzic and co-workers have proposed that the reduction of $[PtCl_6]^{2-}$ to Pt metal is assisted by Ru-OH surface species, easily formed under the specific experimental conditions [Eqs. (2) and (3)].

$$Ru^0 + x\,H_2O \rightarrow RuO_xH_x + 2\,(x-y)H^+ + (2x-y)\,e^- \quad (2)$$

$$[PtCl_6]^{2-} + 4\,e^- \rightarrow Pt^0 + 6\,Cl^- \quad (3)$$

Herein, we describe the synthesis and characterization of new Pd-based catalysts obtained by the spontaneous deposition of Pd on Ni-Zn materials. Also, more traditional Vulcan XC-72-supported Pd catalysts were prepared for comparative purposes. The electrochemical activity of all catalysts towards ethanol oxidation in alkaline media has provided valuable information that has allowed us to develop extremely efficient DEFCs.[35]

Skeletal or sponge nickel alloys similar to Raney nickel (such as Ni-Al and Ni-Zn) have been used for many years to catalyze various chemical processes (e.g. hydrogenation and hydrogenolysis) as well as electrochemical processes, such as the electrolysis of water.[36,37] Skeletal Ni materials have the advantage of being cheap and have a high surface area. However, their characteristic pyrophoricity, hence the great tendency to be oxidized in air with the formation of thick surface-oxide layers and the strong corrosion in acidic conditions, have prevented their effective use in polymer electrolyte membrane fuel cells (PEMFCs) and DMFCs.[38] The alkaline environment is definitely much better for Ni, and the effectiveness of Ni electrocatalysts to oxidize alcohols in alkaline media either in half[39–42] or monoplanar cells[43] has been widely demonstrated. In no case, however, were appreciable power densities obtained.

Our attention to Ni-Zn alloys or composites as active supports for the fabrication of DAFC anode electrocatalysts was attracted by the recent discovery that Raney nickel materials can be successfully employed as supports for noble-metal catalysts to give effective anodes in aqueous ammonia electrolyz-

ers.[44,45] This evidence prompted us to explore more carefully the literature, where we came across a patent from 1997 which claimed the preparation of a catalyst for the oxidation of hydrogen in a fuel cell obtained by the spontaneous deposition of noble metals, including palladium, onto a Ni-Al alloy after the Al was removed by treatment with a strong base.[46] A further advantage of Ni-Zn materials as substrates for spontaneous deposition procedures is just the presence of Zn, which is more electropositive than Ni and therefore prone to undergo transmetalation with Pd^{II} or Pd^{IV}.

The skeletal Ni-based materials used in this study to bring about the spontaneous deposition of palladium are not commercial products. We prepared our own Ni-Zn supports on the basis of the procedures reported for two known materials: the Ni-Zn Urushibara catalysts, which exist in two forms depending on whether the excess of Zn is removed by using an acid or a base,[47] and the Ni-Zn-P composites developed for the protection of steel from corrosion.[48] The latter materials have the characteristic of having a higher nickel content and stability as compared to traditional Raney nickel. To the best of our knowledge, there are no other reports claiming the use of Urushibara-like or Ni-Zn-P composites as supports for manufacturing anode electrocatalysts for DAFCs.

Results and Discussion

Catalyst Synthesis

The spontaneous deposition of Pd was achieved in a straightforward manner by stirring an aqueous solution of K_2PdCl_4 in the presence of either Ni-Zn or Ni particles supported on Vulcan XC-72 under a nitrogen atmosphere. Two different Ni-Zn/C materials were prepared and used as support/reagent for the deposition of Pd. One of these may be classified as a member of the family of the Urushibara catalysts, which consist of highly porous materials obtained by reducing hydrated $NiCl_2$ with Zn powder, followed by treatment of the resulting Ni-Zn phase with an alkaline hydroxide, generally NaOH.[47] The resulting product is herein denoted as Ni-Zn/C. The second Ni-Zn-based support was a Ni-Zn-P/C composite prepared by the reduction of mixtures of Ni and Zn salts with sodium hypophosphite in the presence of sodium citrate and ammonium chloride, followed by treatment with concentrated KOH solution.[48,49] As shown by the energy-dispersive spectroscopy X-ray (EDX) spectrum in Figure 1, the final product, after the deposition of Pd, contained Ni, Zn and P, with a largely prevailing Ni content. The third support was a simple Ni/C material obtained by reducing $Ni(OAc)_2$ adsorbed onto Vulcan XC-72 with $NaBH_4$ in deaerated water.

Note that the amount of Pd deposited onto the Ni-Zn/C or Ni/C materials was, in all cases, proportional to the loss of Ni and Zn from the support, which confirms the occurrence of a redox transmetalation process. Control experiments in which an aqueous solution of K_2PdCl_4 was added to a stirred dispersion of Vulcan XC-72 followed by washing with water did not show any appreciable deposition/adsorption of Pd on the carbon black.

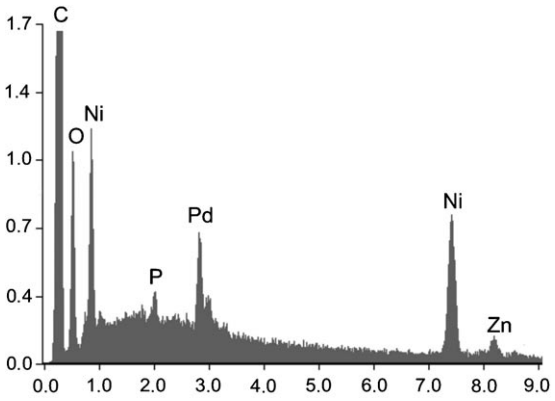

Figure 1. EDX spectrum of a sample of Pd-(Ni-Zn-P)/C.

Finally, the Pd/C catalysts were prepared by electroless reduction in aqueous solution of Vulcan XC-72-impregnated $PdCl_2$/HCl with ethylene glycol at high temperature[50–52] or with $NaBH_4$ at 0–5 °C.[15]

Catalyst Characterization

The morphology and distribution of the supported metal particles in Pd-(Ni-Zn-P)/C, Pd-(Ni-Zn)/C and Pd/C were evaluated by high-resolution transmission electron microscopy (HRTEM), while the relative distribution of Pd and Ni atoms was obtained by combined HRTEM/EDX analysis.

The HRTEM image of Pd-(Ni-Zn-P)/C showed a broad metal particle size distribution, with an overall mean diameter of 3.2 nm and a standard deviation of 1.3 nm (Figure 2a). Selected micrographs of this material are given in Figure 2b. The largest fraction of the metal particles (70% of the total metal amount) was below the main feature of the distribution function (size range of 1–4 nm), corresponding to a mean diameter of about 2.4 nm. These particles were present as particle agglomerates, and their average composition, detected by large-spot in-column EDX, corresponded to Pd/Ni = 1:1. The smallest particles were mainly Ni-containing particles, but no Ni metal crystal plane was resolved. A few lamellar-like Ni metal aggregates were visible. Phosphorus and zinc atoms were everywhere below the sensitivity level of the EDX probe, as expected for a uniform dispersion at such a low concentration of these two elements (0.4 wt% Zn; 0.2 wt% P), while oxygen was uniformly detected all over the sample in moderate concentration. A few larger Pd particles were also visible (4–6 nm) which we attribute to a thick amorphous oxide layer surrounding small metal cores, as no resolved crystal structure was detected.

Most of the carbon support grains were crystalline (with well-resolved diffraction fringes of graphite planes), but the distribution of metal aggregates over the different support regions was quite inhomogeneous.

The particle distribution for the Pd-(Ni-Zn)/C catalyst was quite narrow and peaked around a mean diameter value of 2.3 nm with a standard deviation of 0.5 nm (Figure 3a). Selected micrographs of this material are given in Figure 3b.

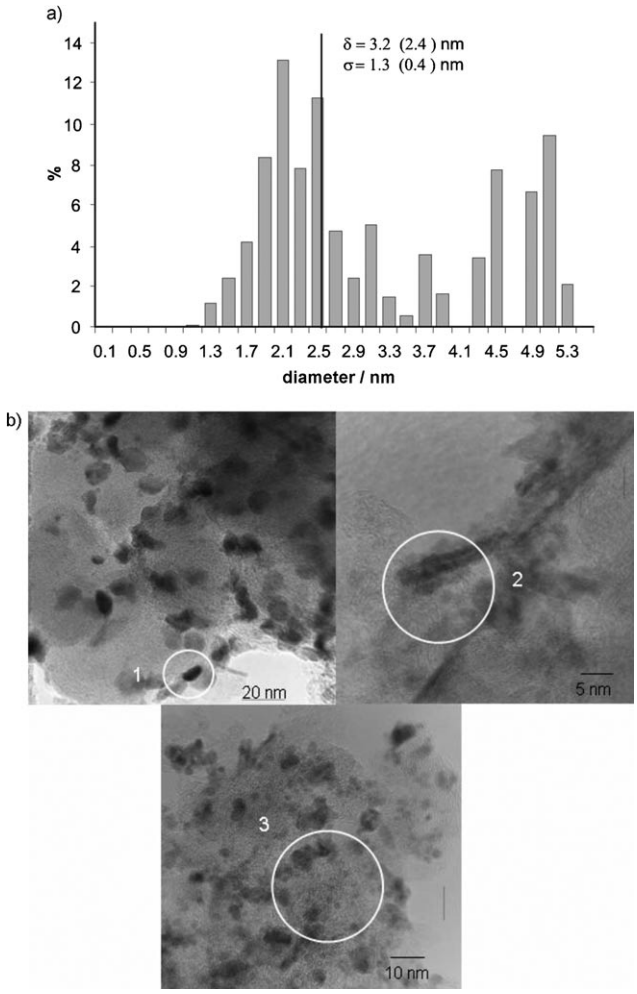

Figure 2. a) HRTEM histograms of particle distribution versus diameter for Pd-(Ni-Zn-P)/C. The average size (δ) and standard deviation (σ) are reported (values corresponding to the main features are reported in parenthesis; see text for details). b) HRTEM images of Pd-(Ni-Zn-P)/C at different magnifications. Spots of EDX analysis are shown in circles; Pd/Ni relative compositions as detected by EDX integrated peak areas: 1) Pd; 2) Ni; 3) Ni/Pd = 1:1: There is a minor O contribution everywhere.

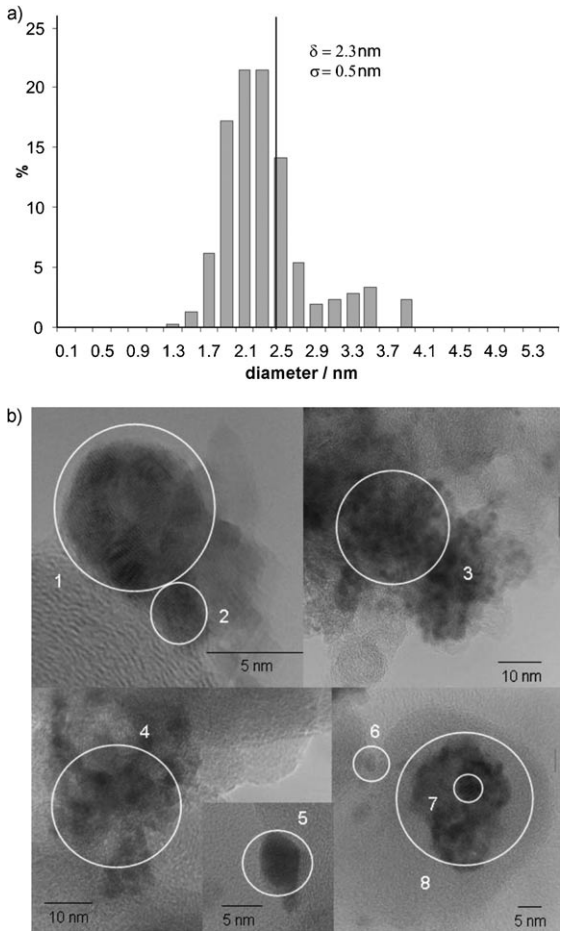

Figure 3. a) HRTEM histograms of particle volume distribution versus diameter for Pd-(Ni-Zn)/C. The average size (δ) and standard deviation (σ) are reported. b) HRTEM images of Pd-(Ni-Zn)/C at different magnifications. Spots of EDX analysis are shown in circles; Pd/Ni relative compositions as detected by EDX integrated peak areas: 1) Ni > Pd with Ni(110) plane fringes; 2) Ni-(111) plane fringes; 3) Pd/Ni = 1:2; 4) Pd/Ni = 1:1; 5) Pd with cuboctahedron crystal facets; 6) Ni; 7) Pd(110) plane fringes; 8) Pd > Ni. There is a minor O contribution everywhere.

The composition of the metal particles was determined with an in-column EDX probe: Pd was mainly detected in correspondence of large aggregates of several small particles with an average molar Pd/Ni ratio of 1:2. In such regions, the oxygen contribution to the EDX signal was also relevant, but several particles, either of Ni or Pd, showed well-defined truncated cuboctahedron-hexagonal geometry habit and diffraction fringes of metal Ni(110) ($d = 0.249$ nm), Ni(111) ($d = 0.203$ nm), Pd(110) ($d = 0.275$ nm) and Pd(200) ($d = 0.194$ nm) crystal planes, in agreement with the Ni and the Pd face-centered cubic (fcc) packing in a cuboctahedral growth geometry. Where the metal particles were sufficiently large and isolated to allow for a single-particle EDX analysis, the composition was predominantly Pd or predominantly Ni-Zn (Zn/Ni ≈ 0.2), with the Pd particles being larger than the Ni particles and not alloyed. Indeed, a comparison of the metal element distribution mapping, performed at low magnification (250 000×) for Pd and Ni, showed clearly the proximity of the particles of these two atomic species, as the distribution density was well reproduced. However, the images were not superimposable, suggesting the absence of alloys or decoration effects.

Most of the support grains were crystalline with well resolved diffraction fringes of the graphite planes and showed a uniform dispersion of the metal particles over the entire support surface.

The HRTEM image of Pd/C, obtained by method A (see Experimental Section), showed quite a broad particle size distribution with a mean diameter of 3.7 nm and a standard deviation of 1.1 nm (Figure 4a). A representative micrograph of this material is given in Figure 4b. The Pd particles were much larger and their crystal habit was much less clearly defined as compared to those in Pd-(Ni-Zn)/C. There was no indication of any resolved crystal structure in any of the images, probably due to the presence of a thick amorphous oxide layer surrounding small metal cores.

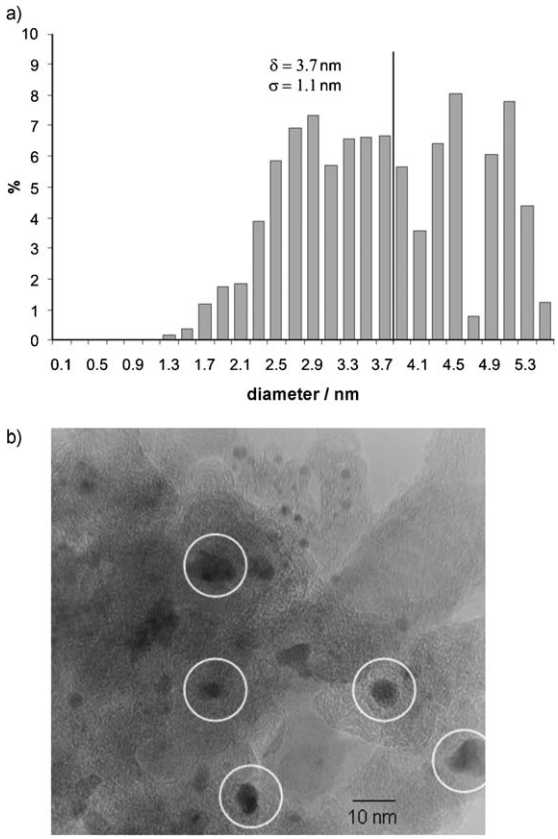

Figure 4. a) HRTEM histograms of particle distribution versus diameter for Pd/C. The average size (δ) and standard deviation (σ) are reported. b) HRTEM images of Pd/C. Regions of EDX analysis (Pd with minor O contribution) are marked by circles.

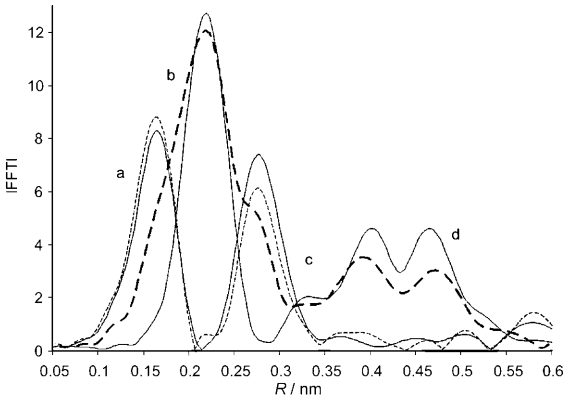

Figure 5. Ni K-edge Fourier transform EXAFS spectra (not phase-corrected): a) Pd-(Ni-Zn-P)/C (——); b) Pd-(Ni-Zn)/C (-----); c) NiO (•••••); and d) Ni foil reference standards (——).

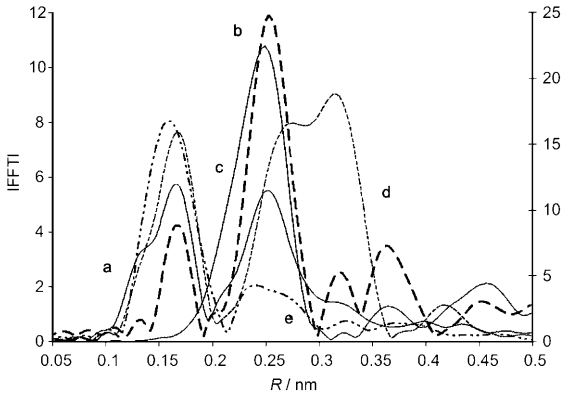

Figure 6. Pd K-edge Fourier transformed EXAFS spectra (not phase-corrected): a) Pd-(Ni-Zn-P)/C; b) Pd-(Ni-Zn)/C; reference standards: c) Pd foil (right axis); d) PdO; and e) $[Pd(acac)_2]$.

EXAFS and XANES Spectra

Samples of Pd-(Ni-Zn-P)/C and Pd-(Ni-Zn)/C were further investigated by extended X-ray absorption fine structure spectroscopy (EXAFS) and near-edge X-ray absorption spectroscopy (XANES) in an attempt to elucidate the local environment of the Pd and Ni atoms in the corresponding agglomerates. The Pd-(Ni-Zn)/C sample was kept under a nitrogen atmosphere throughout, while the Pd-(Ni-Zn-P)/C sample was purposefully exposed to air for 12 h before being subjected to the spectroscopic analysis (the preparation of the catalytic ink and electrodes for the electrochemical characterization was carried out in air). Comparisons of the Fourier transform EXAFS spectra are reported in Figure 5 and Figure 6, while the best fit results for both Ni and Pd K-edges are summarized in Table 1 together with data for Ni and Pd foils, Ni and Pd oxides and $[Pd(acac)_2]$ as reference standards.

The Pd-(Ni-Zn-P)/C sample showed oxidized Ni in a Ni bulk oxide phase, well fitted as a NiO structure (Figure 5), with only small contributions from Zn at distances consistent with Ni-Zn and Ni-P-Zn (Table 2) in many of the possible alloy phases in which they can exist. Pd was present partly in the reduced metal form to give very small metal clusters (<0.5 nm) with an average number of 1.8 Pd–Pd metal neighbors and partly as isolated ions in a four-oxygen coordination sphere (Figure 6). The small dimensions of the Ni particles in the Ni-Zn-P support well account for the observed oxidation of the surface Ni atoms upon exposure to air. The very small Pd clusters together with the isolated Pd ions are consistent with the occurrence of a truly spontaneous deposition process (Scheme 1). The presence of 1.9 Ni atoms at a distance of 3.24 Å from the isolated Pd sites, consistent with a Pd-O-Ni shell, suggests that the Pd single sites are stabilized by the oxygen atoms of the Ni-O layer on the surface of Pd-Ni-Zn-P/C. Several examples of bonding interaction of metal ions with surface oxygen atoms can be found in the surface organometallic chemistry literature.[53] In particular, it was recently reported that Rh^+ ions stabilized by 1,2-bis(diphenylphosphino)propane can be immobilized over silica-supported Pd oxide by a bonding interaction with PdO oxygen atoms.[54]

In the Pd-(Ni-Zn)/C sample, nickel was largely present as small Ni^0 metal particles, with an estimated average size of 1.5 nm (Figure 5), while the large majority of palladium was present as small Pd^0 particles with an average size of 1 nm (XANES spectra in Figure 7), with a very minor contribution from oxidized Pd atoms, most probably, as a Pd oxide layer at the metal particle surface, as also small contributions from the

Table 1. EXAFS best fit results at Ni and Pd K-edges and estimated average metal particle diameters (*D*).[a]

Sample			Ni K-edge		
	shell	N	*R* [Å]	σ_{DW} [Å]	*D* [Å]
Pd-(Ni-Zn-P)/C	Ni-O	5.4(1)	2.04(2)	0.072(2)	
	Ni-Zn	1.3(2)	2.48(3)	0.097(4)	
	Ni-Ni_{ox}	8.9(1)	3.12(2)	0.098(3)	
	Ni-Zn_{NiPZn}	1.5(2)	3.08(3)	0.099(1)	
Pd-(Ni-Zn)/C	Ni-O	2.5(1)	2.02(2)	0.074(2)	
	Ni-Ni_{ox}	3.7(3)	2.96(2)	0.081(3)	15
	Ni-Ni_{met}	5.3(2)	2.46(3)	0.084(1)	
Ni foil	Ni-Ni	12	2.48(1)	0.073(1)	
NiO	Ni-O	6	2.08(2)	0.065(3)	
	Ni-Ni	12	2.94(3)	0.081(2)	
Sample			Pd K-edge		
	shell	N	*R* [Å]	σ_{DW} [Å]	*D* [Å]
Pd-(Ni-Zn-P)/C	Pd-O	4.0(2)	2.02(2)	0.077(4)	
	Pd-Pd_{met}	1.8(3)	2.74(3)	0.071(2)	<5
	Pd-Ni_{ox}	1.9(2)	3.24(3)	0.089(4)	
Pd-(Ni-Zn)/C	Pd-O	3.5(3)	2.05(3)	0.079(2)	
	Pd-Pd_{met}	3.3(4)	2.75(2)	0.070(4)	10
	Pd-Pd_{ox}	1.7(2)	3.38(4)	0.071(2)	
Pd foil	Pd-Pd	12	2.738(1)	0.006(1)	
PdO	Pd-O	4	2.032(2)	0.056(2)	
	Pd-Pd	4	3.042(2)	0.088(3)	
	Pd-Pd	8	3.378(4)	0.089(2)	
$[Pd(acac)_2]$[b]	Pd-O	4	1.963(1)	0.006(2)	

[a] Error bars for the last decimal place are provided in parentheses. Subscripts: ox = oxidized, met = metal. [b] acac = acetylacetonate.

Table 2. Relevant electrochemical parameters for the ethanol oxidation reaction at room temperature on electrodes coated with the catalysts investigated in this work[a] or with previously reported catalysts.

Catalyst	J_p [mA cm^{-2}]	Sa_p [mA µg(Pd)$^{-1}$]	V_p [V]	Q_{sa} [C µg(Pd)$^{-1}$]	Tafel slope [mV]
Pd/C	84.5	3.03	−0.12	0.0136	153 ($\alpha=0.4$)
Pd-(Ni-Zn-P)/C	108.7	3.03	−0.10	0.0135	132 ($\alpha=0.4$)
Pd-(Ni-Zn)/C	78.5	3.60	−0.14	0.0152	140 ($\alpha=0.4$)
Pd/C[b]	21	0.07	0.04		188[c]
Pd-NiO/C[d]	95	0.32	−0.08		195[c]
Pd/TiO_2C[e]	76	0.25	−0.19		
Pd/CPAA[f]	69	0.23	−0.08		

[a] Average values for at least three measurements. Peak current density (J_p), specific peak current density (Sa_p), forward anodic peak potential (V_p), integrated specific charge of the anodic peak area (Qsa), Tafel slopes, and electronic transfer coefficient α. [b] Data taken from ref. [12]. [c] Data taken from ref. [10]. [d] Data taken from ref. [13]. [e] Data taken from ref. [19]. [f] Data taken from ref. [18] (CPAA = carbonized and pulverized porous anodic alumina).

outer PdO shells were detected. However, the presence of isolated Pd ions surrounded by four oxygen atoms cannot be ruled out. There was no evidence for formation of a Ni-Pd alloy phase, as we found neither Ni neighbors at the Pd edge nor Pd neighbors at the Ni edge.

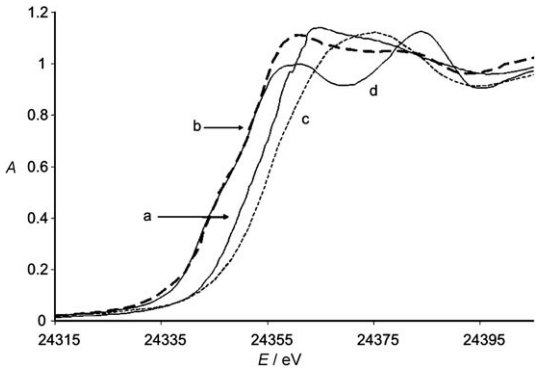

Figure 7. Pd K-edge normalized XANES spectra: a) Pd-(Ni-Zn-P)/C (——); b) Pd-(Ni-Zn)/C (-----); c) PdO (•••••); and d) Pd foil reference standards (——).

XRPD Analysis

The structures of Pd-(Ni-Zn)/C, Pd-(Ni-Zn-P)/C, Pd/C and Pd-Ni/C were investigated by X-ray powder diffraction (XRPD). The patterns of these samples together with those of the corresponding Pd-free supports are provided in Figures 8–11. All spectra showed the typical diffraction peaks of the carbon support at around 25° and 44°. In the samples of materials obtained by the spontaneous deposition procedure, namely Pd-(Ni-Zn)/C and Pd-(Ni-Zn-P)/C (Figure 8 and Figure 9, respectively), the diffraction peaks at the Bragg angles of 40.10°, 46.40°, and 68.08° were readily attributed to the (111), (200), and (220) facets of fcc Pd crystals.[55] In both samples, the peaks were very sharp, which is consistent with the presence of crystalline clusters as confirmed by the EXAFS and HRTEM studies. A contribution from Ni(111) (44.5°) was clearly evident in the spectrum of Pd-(Ni-Zn)/C.[55]

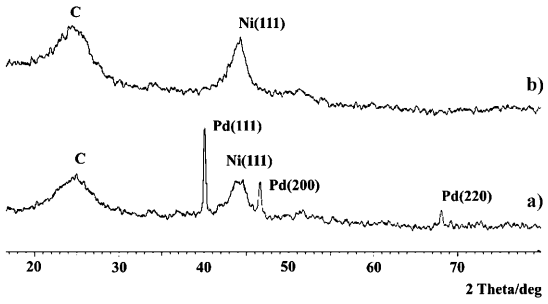

Figure 8. XRD patterns of a) Pd-(Ni-Zn)/C and b) Ni-Zn/C.

The XRPD spectrum of Pd-(Ni-Zn-P)/C (Figure 9a) was more complex than that of Pd-(Ni-Zn)/C. Indeed, in addition to the sharp peaks of fcc Pd, there were several peaks due to the (Ni-Zn-P)/C support at around 19°, 32.8°, 38.2°, 59.0°, and 62.8° (Figure 9b). A reliable assignment of each peak was made difficult by the lack of univocal data in the literature owing to the fact that Ni-Zn-P alloys can exist in a variety of compositions and morphologies depending on the experimental conditions, in particular, the stoichiometric ratio of the reagents and the pH.[48,56–58] Cross experiments on supports containing Zn-P/C

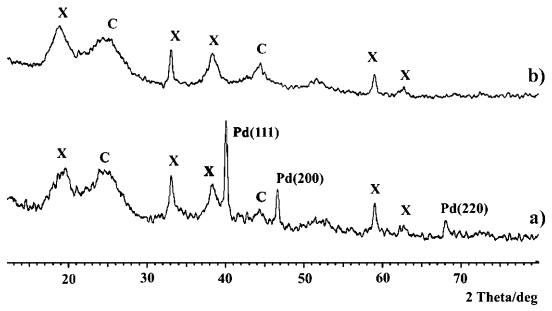

Figure 9. XRD patterns of a) Pd-(Ni-Zn-P)/C and b) Ni-Zn-P/C.

and Ni-P/C phases confirmed that nickel contributes to all the peaks marked "X" in Figure 9.

The Pd particles supported on Vulcan XC-72, prepared by electroless reduction of $PdCl_2$/HCl with ethylene glycol, are clearly much less crystalline but still representative of fcc Pd (Figure 10 a).[55]

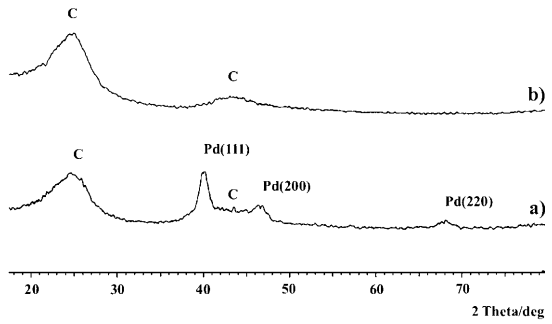

Figure 10. XRD patterns of a) Pd/C and b) C.

The XRPD patterns of Ni/C obtained by electroless reduction of $Ni(OAc)_2$ adsorbed onto Vulcan XC-72 and of Pd-Ni/C obtained by spontaneous deposition of K_2PdCl_4 on Ni/C are shown in Figure 11. The spectrum clearly shows the presence of quite amorphous Pd, while Ni is most likely present as amorphous NiO.

From a comparison of the XRPD spectra reported in Figures 8–11, one may readily conclude that only the supports containing Ni alloyed with Zn or Zn-P allow for the formation of highly crystalline Pd particles (see the EXAFS and HRTEM studies).

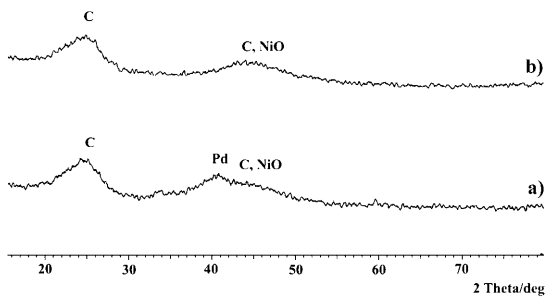

Figure 11. XRD patterns of a) Pd-Ni/C and b) Ni/C.

Electrochemical Characterization of the Support Materials

The electrochemical behavior of the support materials Ni-Zn/C, Ni-Zn-P/C and Ni/C in either neat 2 M KOH or in 2 M KOH containing 10 wt% ethanol was studied by cyclic voltammetry (CV). Indeed, nickel alone[40–43] or in conjunction with other transition metals[56–60] is a proven catalyst for the electro-oxidation of alcohols, including ethanol, in alkaline media. Therefore, we were interested in evaluating the intrinsic electrocatalytic properties of the present Ni-based supports in an attempt to either rule out or establish a co-catalytic effect with Pd.

Figure 12 shows a cyclic voltammogram (at the fifth cycle) of an electrode containing Ni-Zn/C in 2 M KOH solution. The typical peak for the oxidation of $Ni(OH)_2$ to NiO(OH) was observed in the positive sweep at 0.44 V, accompanied by the corresponding reversible reduction at 0.29 V in the reverse scan.[61–64] A sharp reduction peak at −0.30 V was observed in the reverse scan whose assignment is not straightforward. Indeed, the reduction of $Ni(OH)_2$ to Ni^0 generally occurs at lower potentials (ca. −1 V).[63,64] According to a recent study by Henn and co-workers,[62] the reduction step at −0.30 V might be due to the occurrence of a reduced phase of the type NiO_2H_{2-x} with $0 < x < 0.3$, which would lead to an effective $Ni(OH)_2$ state. On the other hand, the nanometer size of the nickel particles on Ni-Zn/C might contribute to shift the $Ni(OH)_2/Ni^0$ potential to more positive values, as occurs for the reduction of nanostructured PdO and $Pd(OH)_2$ (see below).

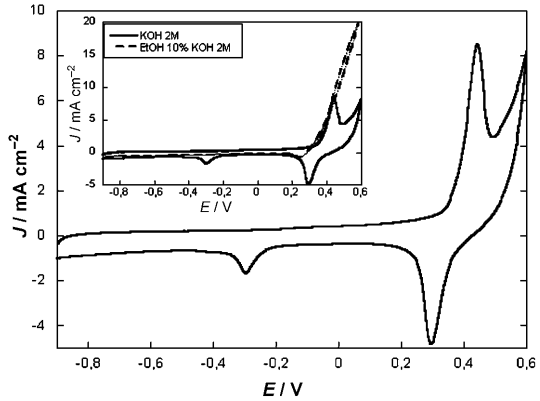

Figure 12. Cyclic voltammogram (*E* vs $Ag/AgCl/KCl_{sat}$) of Ni-Zn/C in 2 M KOH solution. Inset: cyclic voltammogram obtained after adding ethanol (10 wt%; -----) together with that shown in the main picture. Nickel loading: 40 μg cm^{-2}; scan rate: 50 mV s^{-1}.

No current peak in the forward scan attributable to the oxidation of Ni^0 to $Ni(OH)_2$ was observed. This redox process occurs at approximately −0.7/−0.6 V in alkaline media[64] and is difficult to detect owing to its complexity as it involves the formation of α-$Ni(OH)_2$ and its subsequent transformation into β-$Ni(OH)_2$.[61]

The cyclic voltammogram recorded for the same Ni-Zn/C electrode after the addition of ethanol is shown in the inset of Figure 12. As reported by several authors,[41–43] ethanol is oxidized by the reaction with NiO(OH). Consistently, the latter species was removed from the catalyst surface on reaction with ethanol as shown by the disappearance of the two reverse reduction peaks.

A similar but not identical electrochemical behavior was shown by the electrode with the Ni-Zn-P/C material in 2 M KOH (Figure 13). The presence of a different kind of nickel on

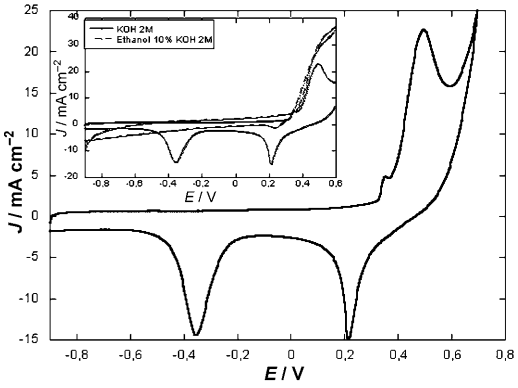

Figure 13. Cyclic voltammogram (*E* vs Ag/AgCl/KCl_{sat}) of Ni-Zn-P/C in 2 M KOH solution. Inset: cyclic voltammogram obtained after adding ethanol (10 wt%; -----). Nickel loading: 55 μg cm^{-2}; scan rate: 50 mV s^{-1}.

the electrode surface was indicated by the higher potential at which $Ni(OH)_2$ was oxidized to NiO(OH) (0.49 V vs 0.44 V) and regenerated by reduction of the latter (0.21 V vs 0.29 V) as well as by the presence of a shoulder at 0.35 V. The reduction peak of the species generated at 0.21 V on the Ni-Zn-P/C electrode, either $Ni(OH)_2$ to Ni^0 or NiO_2H_{2-x} to $Ni(OH)_2$, occurred at slightly more negative potential as compared to the Ni-Zn/C electrode (−0.35 vs −0.30 V). The more complex nature of the Ni-Zn-P/C material, which is an actual Ni-Zn-P alloy,[48,65–67] probably inhomogeneous, may well account for the different polarization values as well as the broadness of the current peaks. On the other hand, as observed for Ni-Zn/C, the addition of ethanol (inset of Figure 13) resulted in the complete disappearance of the NiO(OH) reduction peak in the reverse scan, which is consistent with an effective electrooxidation activity of ethanol.

The electrochemical behavior of the Ni/C material was similar to those of Ni-Zn/C and Ni-Zn-P/C, with a $Ni(OH)_2$/NiO(OH) oxidation peak at 0.46 V and the second reduction peak at −0.30 V. At a comparable metal loading (50 μg cm^{-2}), however, the current peaks of either electron transfer were much lower, which may be due to the different size and morphology of the metal particles on Ni/C prepared by the plain reduction of adsorbed $Ni(OAc)_2$ with $NaBH_4$.

In view of the fact that the electrochemical oxidation of ethanol on the Pd-containing catalysts occurs at a much lower potential (onset at ca. −0.6 V with a peak current density at ca. −0.1 V; see below), one may safely conclude that the Ni-Zn-based supports, though featured by the capacity to oxidize ethanol in alkaline media, are not directly involved in the ethanol oxidation reaction occurring at the largely negative potentials of the Pd-containing catalysts (see below).

Electrochemical Characterization of the Pd-Based Catalysts in KOH Solution

The CV behavior of Pd-(Ni-Zn)/C, Pd-(Ni-Zn-P)/C, and Pd/C was investigated in 2 M KOH solution with Pd loadings between 22.13 and 26.94 μg cm^{-2}, as these experimental parameters were successively used to study the electrochemical oxidation of ethanol (see below). In the cyclic voltammogram of Pd/C in KOH solution (Figure 14a), the forward scan shows a very broad oxidation wave starting at about −0.2 V with a peak at 0.1 V, while a much narrower and more intense reduction peak is observed in the reverse scan with an onset potential of

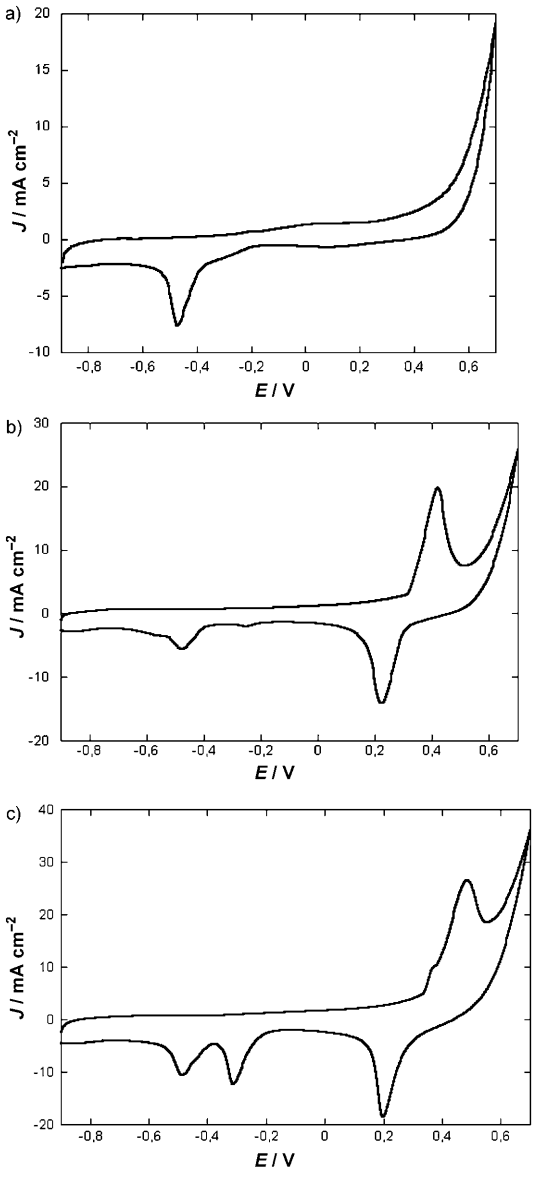

Figure 14. Cyclic voltammograms (*E* vs Ag/AgCl/KCl_{sat}) of a) Pd/C, b) Pd-(Ni-Zn)/C, and c) Pd-(Ni-Zn-P)/C in 2 M KOH solution. Scan rate: 50 mV s^{-1}.

around −0.2 V and a peak at −0.47 V. The position and shape of this reduction wave are consistent with the reduction of nanostructured Pd^{II} species, either PdO or $Pd(OH)_2$. Indeed, in the range of potentials investigated, the formation of Pd^{IV} species can be ruled out.[68,69] Previous CV studies of electrodes coated with either PdO or nanostructured Pd in NaOH solution consider the redox chemistry of these species as a quite complicated process owing to the number of possible oxide/hydrous oxide/hydroxy surface species,[68,70] which would explain the broad shape of the reduction wave.

The cyclic voltammograms of Pd-(Ni-Zn)/C and Pd-(Ni-Zn-P)/C in 2 M KOH solution are shown in Figure 14b and c, respectively. The CV responses for either material can be assimilated to the sum of the trace of Pd/C (Figure 14a) with the traces recorded for the Ni-based supports (Ni-Zn/C and Ni-Zn-P/C, Figure 12 and 13, respectively), which is an indirect confirmation that Pd and Ni are not alloyed in either material.

Electrochemical Oxidation of Ethanol by the Pd-Based Catalysts

The electrochemical activity of Pd-(Ni-Zn)/C, Pd-(Ni-Zn-P)/C, and Pd/C for ethanol oxidation was investigated by CV at room temperature. A preliminary study was carried out to find out suitable conditions in terms of catalyst loading on the electrode as well as KOH and ethanol concentrations. For all catalysts, Pd loadings varying from 20 to 25 $\mu g\,cm^{-2}$, corresponding to 18–20 mg of ink, gave the highest current density values for the oxidation of ethanol (10 wt%) in 2 M KOH at a scan rate of 50 $mV\,s^{-1}$.

A series of cyclic voltammograms recorded at KOH concentrations spanning from 0.001 to 4 M showed the generation of the highest current densities in the range 1–1.5 M KOH. However, all the following electrochemical studies, either in half cells (reported in this work) or in monoplanar cells,[35] were carried out using a 2 M KOH solution to keep the concentration of OH^- as constant as possible throughout the course of the experiment. Indeed, the oxidation of ethanol in alkaline media consumes OH^- groups, irrespective of the oxidation level of the substrate (acetate or carbonate) [Eqs. (4) and (5)]. At this point, it is worth stressing the results of a study where electrodes catalyzed with Pd-(Ni-Zn)/C, Pd-(Ni-Zn-P)/C, and Pd/C were used as anodes in both passive and active monoplanar DEFCs equipped with anion-exchange membranes.[35] Irrespective of the anode catalyst, ethanol was selectively converted into (potassium) acetate according to Equation (4).

$$C_2H_5OH + 5\,OH^- \rightarrow CH_3COO^- + 4\,H_2O + 4\,e^- \quad E^\circ = -0.743\ V \tag{4}$$

$$C_2H_5OH + 16\,OH^- \rightarrow 2\,CO_3^{2-} + 11\,H_2O + 12\,e^- \quad E^\circ = -0.724\ V \tag{5}$$

Finally, the oxidation of ethanol was studied with each catalyst in 2 M KOH solution, varying the substrate concentration from 0.1 to 8 M. A good response in terms of current density was obtained with a 2 M solution of ethanol, which corresponds to around 10 wt% (2.17 M). Higher ethanol concentrations, although yielding better results, were not considered for minimizing the alcohol crossover in real DEFCs. Indeed, it is generally found that at concentrations higher than 10 wt%, the alcohol crossover becomes relevant for most polymer ion-exchange membranes with consequent high cell overvoltages and decreased efficiency due to loss of fuel by evaporation from the cathode compartment.[71,72]

Thus, all the CV measurements reported below were performed at a sweep rate of 50 $mV\,s^{-1}$ in deoxygenated 10 wt% ethanol/2 M KOH solutions and electrodes containing a Pd loading between 22 and 25 $\mu g\,cm^{-2}$.

Figure 15 shows the cyclic voltammograms of the ethanol oxidation reaction on Pd/C, Pd-(Ni-Zn-P)/C, and Pd-(Ni-Zn)/C electrodes. Relevant electrochemical parameters, such as peak

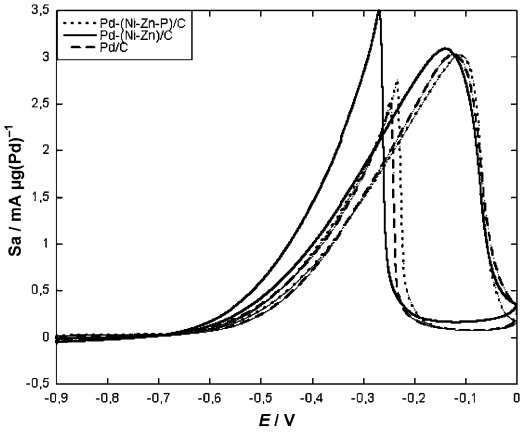

Figure 15. Cyclic voltammograms (at the tenth cycle; *E* vs $Ag/AgCl/KCl_{sat}$) of ethanol oxidation on Pd/C, Pd-(Ni-Zn-P)/C, and Pd-(Ni-Zn)/C electrodes in 2 M KOH and 10 wt% ethanol. Scan rate: 50 $mV\,s^{-1}$.

current density (J_p), specific peak current density (Sa_p), forward anodic peak potential (V_p), integrated specific charge of the anodic peak area (Qsa), and Tafel slopes, together with the electronic transfer coefficient α, are listed in Table 2. The three catalysts showed high activity for the ethanol oxidation reaction with onset potentials of around −0.6 V and specific current densities higher than 3 $mA\,\mu g(Pd)^{-1}$, which are remarkable results indeed. In fact, we are not aware of such a performance in ethanol oxidation with any known electrocatalyst especially at the very low metal loadings used in this work.

As shown by the traces in Figure 15, the electrocatalyst Pd-(Ni-Zn)/C was slightly more active than either Pd-(Ni-Zn-P)/C or Pd/C, especially in terms of forward and backward anodic peak potentials as well as specific peak current density. As all catalysts exhibited a slow but constant decrease of the peak back current with increase of the anodic limit (from −0.1 to 0.6 V), the backward scan peak can be associated to the oxidation of both freshly chemisorbed ethanol (prevalent contribution) and weakly adsorbed species,[73] most likely Pd-acetyl species whose oxidative reaction with OH_{ads} is believed to generate CH_3COOH.[2]

The only comparable electrochemical results for ethanol oxidation are those reported by Shen et al. for a family of Pd-based electrocatalysts containing significantly higher metal loading (300 $\mu g\,cm^{-2}$) and promoted by metal oxides supported on various conductive materials (Vulcan XC-72R,[10,12,13] carbonized TiO_2 nanotubes,[19] carbonized porous anodic alumina[18]). Selected data reported by Shen et al. are provided in Table 2. From the data listed in Table 2 and considering the very low Pd loadings (from 22 to 25 $\mu g\,cm^{-2}$), one readily sees that Pd/C, Pd-(Ni-Zn-P)/C, and Pd-(Ni-Zn)/C can be classified among the most active electrocatalysts ever reported for the ethanol oxidation reaction. Note also that the present Pd/C catalyst is much more active for ethanol oxidation than that described by Shen et al. (Table 2). We are inclined to ascribe the higher electrochemical activity of the present Pd/C catalyst to the higher dispersion of its metal particles (4 nm vs 10 nm in Pd/C_{Shen}[10,12]). Indeed, quite different procedures were adopted to prepare the two catalysts (reduction of $PdCl_2$/HCl with ethylene glycol for Pd/C vs reduction with $NaBH_4$ for Pd/C_{Shen}).

Tafel plots for the ethanol oxidation reaction on the Pd/C, Pd-(Ni-Zn-P)/C, and Pd-(Ni-Zn)/C electrodes were obtained at a scan rate of 5 $mV\,s^{-1}$ in the potential interval from −0.7 to −0.6 V (2 M KOH, 10 wt% ethanol). The values for the Tafel slopes and of the α coefficients (Table 2) are comparable with each other as well as with those reported by Shen et al. for the Pd/C electrocatalyst promoted by nanocrystalline metal oxides.[10] The Tafel slopes indicate the same reaction mechanism, while the α parameter of 0.4 is consistent with an electrochemical rate-limiting step for the ethanol oxidation reaction. As for the absolute values of the Tafel slopes, the relatively high values observed are in line with porous high-surface-area electrodes with high electrocatalytic activity.[10,70]

The performance stability of the electrocatalysts for ethanol oxidation was investigated by chronopotentiometry. Steady-state measurements were carried out with a constant current density polarization of 3 $mA\,cm^{-2}$. Figure 16 shows the relative chronopotentiometric traces for experiments lasting 5.5 h. For all electrocatalysts, there was some potential oscillation in the first 2–3 h of ethanol oxidation, then no oscillation at all, as well as a potential increase by only a few tens of mV after 5.5 h. Both features suggest the absence of effective catalyst deterioration, for example, by the formation of strongly adsorbed species on the catalyst surface. Catalyst poisoning in alcohol electrooxidation is generally related to strong adsorption of CO and CO-like species.[1,2,6] The fact that no oxidation of ethanol to CO occurs with the present catalysts, which are selective for acetate formation, can account for their remarkable stability. The exclusive formation of acetate ions was confirmed by ionic chromatography analysis of the chronopotentiometric solutions. As previously mentioned, Pd-(Ni-Zn-P)/C, Pd-(Ni-Zn)/C, and Pd/C are being used to fabricate anodes for DEFCs, where ethanol is selectively converted into acetate ion according to Equation (6).[35]

$$C_2H_5OH + O_2 + OH^- \rightarrow CH_3COO^- + 2\,H_2O \qquad (6)$$

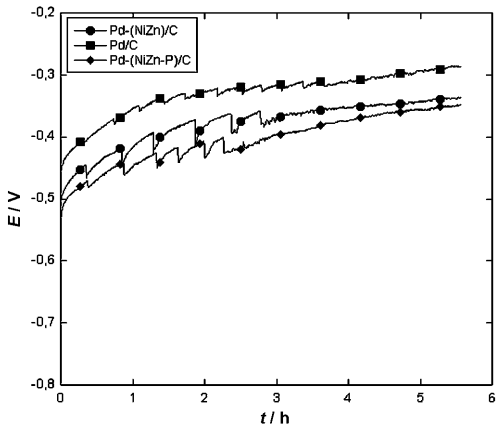

Figure 16. Chronopotentiometric traces of ethanol oxidation on Pd/C, Pd-(Ni-Zn-P)/C, and Pd-(Ni-Zn)/C electrodes at 3.0 $mA\,cm^{-2}$ in 2 M KOH and 10 wt% ethanol.

The best performance stability was provided by the electrocatalysts obtained by the spontaneous deposition procedure, namely Pd-(Ni-Zn-P)/C and Pd-(Ni-Zn)/C. The small increase in the response potential might be due to a number of factors at the electrode interface, such as 1) the increased viscosity of the solution, resulting in a slower diffusion rate of ethanol, 2) the decreased concentration of OH^- anions, and 3) the competitive adsorption of the acetate ion on the active metal sites.

For all electrodes, the anodic peak current density for ethanol oxidation was plotted against the square-root of the scan rate (Figure 17–19). As shown in Figure 17, a linear relationship, typical of an electrochemical reaction under diffusion control, was found for the Pd-(Ni-Zn-P)/C electrode at scan rates lower than 100 $mV\,s^{-1}$. Above this scan rate, the slope decreased tending to a plateau, as if the peak current density were independent of the voltage scanning frequency. Apparently, at scan rates higher than 100 $mV\,s^{-1}$, the ethanol oxidation reaction on Pd-(Ni-Zn-P)/C is limited by other factors than substrate diffusion, for example, the very low density of catalytic centers due to the extremely low Pd loading (22–25 $\mu g\,cm^{-2}$; see below) as well as the desorption of the oxidation product.

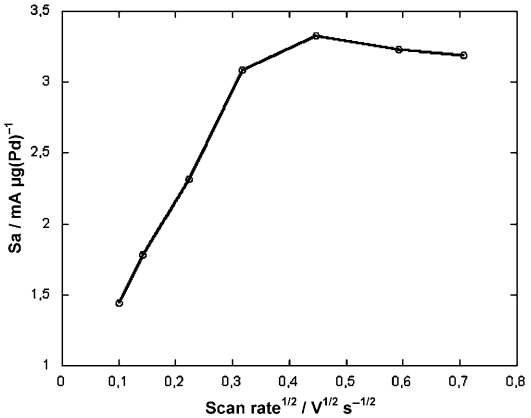

Figure 17. Plot of the anodic peak current density against the square-root of the scan rate for the Pd-(Ni-Zn-P)/C electrode.

The Sa_p versus $V^{1/2}s^{-1/2}$ plot obtained for the Pd-(Ni-Zn)/C electrode is shown in Figure 18. An inital linear correlation below the scan rate of 50 $mV\,s^{-1}$ was followed by a second

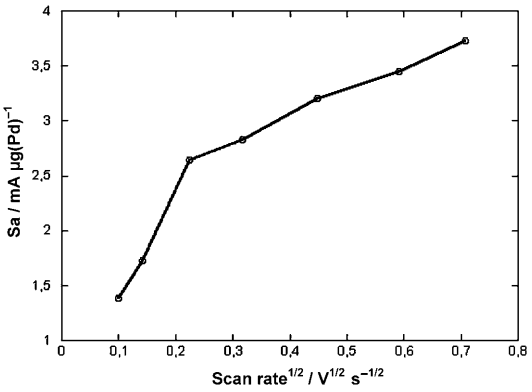

Figure 18. Plot of the anodic peak current density against the square-root of the scan rate for the Pd-(Ni-Zn)/C electrode.

linear correlation with, however, a lower slope. This experimental evidence may be interpreted by assuming that the oxidation of ethanol on the Pd-(Ni-Zn)/C electrode is diffusion-controlled over the range of scan rates investigated, yet with different impact on the reaction rate depending on the scan rate. In other words, at scan rates higher than 50 $mV\,s^{-1}$, the reaction would be still diffusion-controlled but not as effectively as occurs for lower scan rates. A similar behavior has been previously reported for the oxidation of ethanol on Pt electrodes in alkaline media and ascribed to the formation of a passive layer during the early stages of the electron transfer.[39] In the case of Pd-(Ni-Zn)/C, the CV and chronopotentiometric studies seem to exclude electrode passivation, yet the catalyst, being very active, would also generate a very high instantaneous concentration of acetate ion on the surface, with consequent slowing down of substrate adsorption at high scan rates.

The Sa_p versus $V^{1/2}s^{-1/2}$ plot for the ethanol oxidation on the Pd/C electrode is shown in Figure 19. An unambiguous linear dependence of the peak current density on the square-root was not evident for scan rates lower than 50 $mV\,s^{-1}$. Quite similar Sa_p versus $V^{1/2}s^{-1/2}$ plots were reported by Shen et al. for Pd supported on carbonized TiO_2 nanotubes (Pd/TiO_2C_{Shen})[19] and Pd supported on carbonized and pulverized porous anodic alumina ($Pd/CPAA_{Shen}$).[18] In either case, the parabolic shape of the curve at lower scan rates was ascribed to the prevailing occurrence of activation polarization.

An experimental confirmation of the influence of the Pd loading on the shape of the Sa_p versus $V^{1/2}s^{-1/2}$ plots was provided by a Pd/C electrode containing 130 $\mu g\,cm^{-2}$ of Pd, which is about six times higher than that in the catalytic systems studied in this work. As shown by the plot in the inset of Figure 19, the ethanol oxidation was diffusion-controlled over the range of scan rates investigated.

The different shapes of the Sa_p versus $V^{1/2}s^{-1/2}$ plots provided by the Pd-(Ni-Zn-P)/C, Pd-(Ni-Zn)/C, and Pd/C electrodes reflect the different chemical-physical nature of the electrocatalysts. In particular, it is worth recalling that the active Pd sites in Pd-(Ni-Zn)/C and Pd-(Ni-Zn-P)/C are dispersed on a nickel phase supported on the carbon black prior to Pd deposition. In contrast, the Pd sites in Pd/C are directly dispersed on Vulcan, hence they might be more easily accessible to the substrate than those in Pd-(Ni-Zn)/C and Pd-(Ni-Zn-P)/C, which would account for the better mass transport properties of the Pd/C electrode.

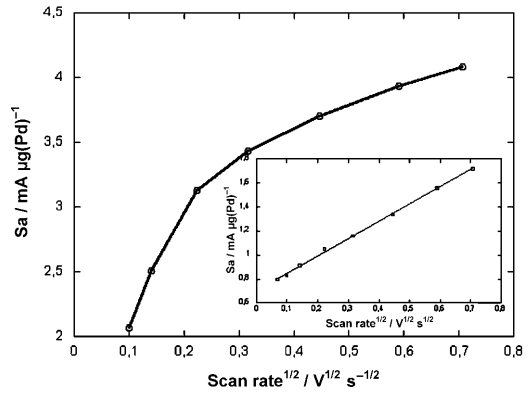

Figure 19. Plot of the anodic peak current density against the square-root of the scan rate for the Pd/C electrode.

Conclusion

In summary, we have shown that Ni-Zn and Ni-Zn-P alloys supported on a conductive carbon black (Vulcan XC-72) are effective materials for the spontaneous deposition of palladium through redox transmetalation reactions. The materials obtained, Pd-(Ni-Zn)/C and Pd-(Ni-Zn-P)/C, were characterized by a variety of techniques, including HRTEM, EXAFS, EDX, ICP-AES, XANES, and XRPD. The analytical and spectroscopic data allowed us to conclude that the surface of Pd-(Ni-Zn)/C and Pd-(Ni-Zn-P)/C contain very small (0.5–1 nm), highly dispersed, and crystalline palladium clusters as well as single palladium sites, likely stabilized by interaction with oxygen atoms from Ni–O moieties.

Electrodes coated with the Pd-(Ni-Zn)/C and Pd-(Ni-Zn-P)/C materials, containing very low Pd loadings (22–25 $\mu g\,cm^{-2}$), were studied for the oxidation of ethanol in alkaline media in half cells. On the basis of the results of an in-depth CV study, we state that the present electrocatalysts exhibit unrivalled activity for the ethanol oxidation reaction with specific currents as high as 3600 $A\,g(Pd)^{-1}$ at room temperature and onset potentials as low as −0.6 V (vs $Ag/AgCl/KCl_{sat}$).

The ethanol oxidation reaction on a nanostructured Pd/C catalyst, prepared by reduction of an aqueous solution of $PdCl_2$/HCl with ethylene glycol in the presence of Vulcan XC-72, was investigated by CV under conditions comparable to those of Pd-(Ni-Zn)/C and Pd-(Ni-Zn-P)/C. The results obtained in the half cell, especially in terms of specific current and onset oxidation potential, were only slightly inferior to those obtained with Pd-(Ni-Zn)/C and Pd-(Ni-Zn-P)/C, but the chronopotentiometric tests showed higher overpotentials. Later tests in both passive and active DEFCs[35] containing anion-exchange

membranes confirmed that the Pd-(Ni-Zn)/C and Pd-(Ni-Zn-P)/C anodes are much more stable and active than the simple Pd/C anode, especially at temperatures below 50 °C.[35]

The size, dispersion, and morphology of the Pd clusters as well as the presence of single Pd sites may well account for the excellent electrocatalytic performance of Pd-(Ni-Zn)/C and Pd-(Ni-Zn-P)/C, which, as a whole, are better catalysts than Pd/C, where the Pd particles are larger, less dispersed, and quite amorphous. In view of the CV experiments in KOH solution with electrodes coated with the Ni-Zn/C and Ni-Zn-P/C supports, prior to and after addition of ethanol (see above), any direct role of the Ni support on the ethanol oxidation reaction at the potentials shown by Pd-(Ni-Zn)/C and Pd-(Ni-Zn-P)/C seems highly unlikely. However, one cannot exclude the existence of a co-catalytic effect of the Ni support on the Pd-catalyzed oxidation reaction of ethanol. Indeed, several researchers have observed that the presence of Ni has a beneficial effect on the electrooxidation of alcohols on late transition metals in either acidic or alkaline media.[56–60] As for Pd catalysts, Shen et al. have shown that the addition of NiO increases remarkably the activity and stability of carbon-supported Pd nanoparticles for the electrooxidation of ethanol in alkaline media.[10,12] Although no clear-cut explanation has been offered so far, it is generally believed that a key role should be played by the capacity of Ni and NiO to generate surface Ni–OH moieties at low potential. Increasing the amount of OH_{ads} on the catalyst surface would actually favor the formation of acetate by coupling with $CO(CH_3)_{ads}$.[2] In turn, the greater oxophilicity of Ni as compared to Pd and the higher binding affinity of Ni towards the acetate ion may facilitate acetate desorption from the active Pd sites, thus accounting for the higher stability of the Pd-(Ni-Zn)/C and Pd-(Ni-Zn-P)/C catalysts even at high ethanol conversion.[35] Current studies in our laboratories are presently aimed at elucidating as many mechanistic facets as possible involved in the oxidation of ethanol to acetate by the present catalysts.

Finally, it is worth commenting that the partial oxidation of ethanol to acetate ion might represent an obstacle to the use of the present Pd catalysts to fabricate stacks of DEFCs capable of delivering kilowatts of energy. However, the good response observed at room temperature in passive monoplanar cells, up to 60 mW cm^{-2} at 0.3 V,[35] presages an effective application in the field of small generators for portable electronics and first-aid devices.

Experimental Section

Materials and General Instrumentation: All manipulations, except as stated otherwise, were routinely performed under a nitrogen atmosphere using standard airless technique. Carbon black (Vulcan XC-72 pellets) was purchased from Cabot Corp., USA. All metal salts and reagents were purchased from Aldrich and used as received. All the solutions were freshly prepared with doubly distilled deionized water. The product analysis of the chronopotentiometic solutions was obtained by ionic chromatography using a Metrohm 761 Compact instrument equipped with a Metrosep Organic Acids column. The sonication process was carried out with a Bandelin Sonopuls probe instrument.

Preparation of Pd-(Ni-Zn-P)/C: $NiSO_4 \cdot 6H_2O$ (3.51 g, 13.35 mmol), $ZnSO_4 \cdot 7H_2O$ (2.03 g, 7.05 mmol), NaH_2PO_2 (3.3 g, 37.5 mmol), $Na_3C_6H_8O_7 \cdot 2H_2O$ (8.56 g, 97.3 mmol), and NH_4Cl (5.2 g, 97.3 mmol) were introduced, in sequence, into a 250 mL three-necked round-bottomed flask containing distilled water (100 mL). The pH of this solution was adjusted to pH 10 with an aqueous solution of KOH (1 M), and then Vulcan XC-72 (6.2 g) was added with stirring to the resulting green-blue solution. After sonication for 20 min, this slurry was heated to reflux temperature for 2 h and then cooled to room temperature. KOH flakes (10 g) were then added, and the mixture was refluxed for 1 h then cooled to room temperature for product filtration. The collected product was washed with distilled water to neutral pH. A small portion of this product was dried by means of a stream of nitrogen and analyzed by ICP-AES (wt%): Ni 10.90, Zn 0.61. The product was suspended in water (150 mL), and the resulting mixture was sonicated for 30 min. A solution of K_2PdCl_4 (1.0 g, 3.06 mmol) in water (250 mL) was slowly added to this suspension, and the resulting suspension was stirred for 30 min at room temperature. The solid product was filtered off, washed several times with distilled water, and finally dried under vacuum at 40 °C until constant weight. Yield: 6.2 g. ICP-AES (wt%): Pd 4.73, Ni 7.45, Zn 0.43. EDX analysis (wt%): Pd 4.9, Ni 7.0, Zn 0.5, P 0.2.

Preparation of Pd-(Ni-Zn)/C: A slurry of Zn powder (2.8 g, 43 mmol) and Vulcan XC-72 (6.0 g) in H_2O (40 mL) in a 100 mL three-necked round-bottomed flask was sonicated for 20 min. The slurry was heated to 90 °C, and then a solution of $NiCl_2 \cdot 6H_2O$ (5.06 g, 21.28 mmol) in water (10 mL) was added within 1–2 min under vigorous stirring. Foaming was observed owing to gas evolution that gradually disappeared in 3–4 min. The resulting reaction mixture was stirred at room temperature for 30 min, then the solid product was filtered off and washed portionwise with hot water (50 °C; 200 mL). This solid was suspended in an aqueous solution of NaOH (13 wt%; 300 mL), and the suspension was stirred for 40 min until no H_2 gas evolution was evident. The final product was separated from the reaction mixture by filtration and washed with distilled H_2O to neutral pH. A small portion of this product was dried with a stream of nitrogen and analyzed by ICP-AES (wt%): Ni 14.4, Zn 3.4. The solid product was suspended in water (400 mL), and the resulting slurry was sonicated for 30 min. A solution of K_2PdCl_4 (1 g, 3.01 mmol) in water (250 mL) was slowly added (ca. 3 h) to this suspension under vigorous stirring, and the reaction mixture was gently stirred overnight at room temperature. The final product was filtered off, washed with water (4×100 mL), and dried at 40 °C under vacuum to constant weight. Yield: 6.0 g. ICP-AES (wt%): Pd 6.4, Ni 9.7, Zn 2.6.

Preparation of Pd-Ni/C: A slurry of Vulcan XC-72 (4 g) and $Ni(OAc)_2 \cdot 4H_2O$ (3.34 g, 13.42 mmol) in water (300 mL) was sonicated for 20 min. Solid $NaBH_4$ (7.6 g, 200 mmol) was added in small portions within 30 min to this suspension under vigorous stirring. The resulting reaction mixture was stirred at room temperature for 2 h, then the solid product was filtered off and washed several times with distilled water. A small portion of this product was dried with a stream of nitrogen and analyzed by ICP-AES (wt%): Ni 16.7. The product was suspended in water (400 mL), and the resulting slurry was sonicated for 30 min. A solution of K_2PdCl_4 (0.7 g, 2.14 mmol) in water (250 mL) was slowly added (ca. 2 h) to this suspension under vigorous stirring, and the reaction mixture was gently stirred overnight at room temperature. The final product was filtered off, washed with water (4×100 mL), and dried at 40 °C under vacuum to constant weight. Yield: 4 g. ICP-AES (wt%): Ni 12.5, Pd 4.4.

Preparation of Pd/C: Method A: Vulcan XC-72 (5.94 g) was sonicated for 20 min in a 500 mL three-necked round-bottomed flask containing ethylene glycol (250 mL). An aqueous solution (50 mL) obtained by treatment of $PdCl_2$ (0.6 g, 3.38 mmol) with 6 mL of HCl (37% w/w) was added dropwise to the resulting dispersion with stirring. After addition of the Pd salt was complete, a solution of NaOH (5.1 g) in water (10 mL) was introduced into the reactor, which was then heated to 140 °C under a nitrogen atmosphere. After 3 h, the reaction mixture was allowed to cool to room temperature and the solid product was filtered off and washed with distilled water to neutral pH. The final product was dried at 40 °C under vacuum to constant weight. Yield: 5.8 g. ICP-AES (wt%): Pd 5.2. Method B: Vulcan XC-72 (4.14 g) was sonicated for 20 min in a 1 L three-necked round-bottomed flask containing water (350 mL). An aqueous solution (150 mL) obtained by treatment of $PdCl_2$ (1.38 g, 7.76 mmol) with 6 mL of HCl (37% w/w) was added dropwise to this dispersion with stirring. The resulting suspension was cooled to 5 °C, then solid $NaBH_4$ (5.88 g, 155 mmol) was slowly added in small portions under vigorous stirring. After stirring at room temperature for 1 h, the solid was filtered off and washed with distilled water to neutral pH. The final product was dried at 40 °C under vacuum to constant weight. Yield: 4 g. ICP-AES (wt%): Pd 20.1.

EXAFS and XANES measurements were carried out at the XAFS beamline of the Elettra synchrotron facility in Basovizza (Trieste), by means of a double-crystal Si(111) monochromator at the Ni K-edge and of Si(311) at the Pd K-edge (synchrotron ring operating at 2.4 GeV). All samples were measured in transmission mode at room temperature at both metal edges. Data were analyzed with the FEFF8 software package.

HRTEM images were recorded with a JEOL Jem-2010 EX microscope. The instrument was equipped with an in-column EDX Spectrometer (probe spot 5 nm, sensitivity 0.5%). Pictures were taken at 250 000–1 200 000× magnifications, spanning wide regions of several support grains in order to provide a representative map of the catalyst system. The samples were ground, and the powders were dispersed in isopropyl alcohol. A drop of each suspension was deposited on the carbon grid, which, after solvent evaporation under vacuum, was inserted in the column of the microscope.

The metal content in all catalysts was determined by inductively coupled plasma atomic emission spectroscopy (ICP-AES) with an Intrepid Iris instrument (Thermo Elemental). Each sample (20–50 mg) was treated in a microwave-heated digestion bomb (Milestone, MLS-200) with concentrated HNO_3 (1.5 mL), 98% H_2SO_4 (2 mL), and a pellet (0.4 g) of a digestion aid reagent (0.1% Se in K_2SO_4). The solutions were analyzed after the carbon residue was filtered off.

EDX was employed to analyze Pd-(Ni-Zn-P)/C. The measurements were performed on untreated powder samples directly deposited on specimen stubs covered with a conductive carbon adhesive, using a FEI Quanta200 microscope operating at 20 KeV accelerating voltage in the low-vacuum mode (0.8 torr).

X-ray powder diffraction spectra were acquired at room temperature with a Bruker D8-Advance diffractometer, employing $Cu_{K\alpha}$ radiation ($\lambda = 1.5418$ Å) in the range between 2.5 and 80.0° and using an acquisition step of 0.030° s^{-1}.

Electrochemical Measurements: The cell used for the cyclic voltammetry experiments was a Kelef cylinder with an inner diameter of 7.2 mm and an outer diameter of 50 mm (Figure 20). The inner volume of the cell was about 1 mL. The working electrode, Glassy Carbon (Sigradur G; 0.867 cm^2), covered by the catalyst, was housed in a special cavity at the top end of the cylinder, and the counter electrode was a gold disc placed at the bottom end. The solution contained in a Pyrex flask was previously deareated by bubbling N_2 and then flushed into the cell at a pressure as low as 0.3 bar N_2. This pressure was applied until the cell was completely filled and then stopped. The inlet and the outlet for the solutions were placed on the side walls of the cell. The inlet was inclined towards the counter electrode so as to allow the solution to gradually fill the cell up and gently wet the working electrode without disturbing the catalyst layer. The electrical contact with the working electrode was secured with two stainless steel screw terminals. Leakage was avoided by pressing both the working and the counter electrode against a suitable silicone O ring. The reference electrode, a miniaturized $Ag/AgCl/KCl_{sat}$ electrode, was placed on the outlet tubing. This allocation allows contamination to be avoided and at the same time is sufficiently close to the working electrode to reduce the uncompensated resistance. All CV studies were carried out using a Parstat 2277 potentiostat-galvanostat (Princeton Applied Research).

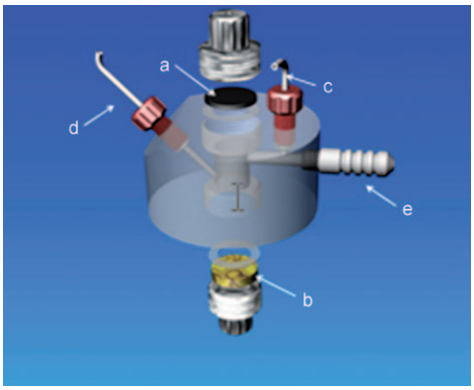

Figure 20. Electrochemical cell for CV experiments: a) working electrode, b) counter electrode, c) reference electrode, d) inlet, and e) outlet.

Ink Preparation: A portion of each electrocatalyst (about 45 mg) was introduced into a 5 mL high-density polyethylene container together with water (1.01 g), KOH (99.99%, Sigma–Aldrich, 65 mg), absolute ethanol (99.8%, Fluka; 0.50 g), and 5% Nafion ion-exchange resin (Sigma–Aldrich; 0.37 g) in ethanol solution. The resulting suspension was sonicated for 30 min with a Branson 3200 bath. Each suspension was freshly prepared just before carrying out the experiment scheduled. The metal loading on each electrode was determined by weighting the amount of ink deposited on the glassy carbon disk.

Acknowledgements

ACTA SpA, the Italian Ministry of Research (FISR project "Nanosistemi inorganici ed ibridi per lo sviluppo e l'innovazione di celle a combustibile), Ente Cassa di Risparmio di Firenze (HYDROLAB project), and the European Commission (Network of Excellence IDECAT (contract no. NMP3-CT-2005-011730) are gratefully acknowledged for financial support. The ELETTRA synchrotron light laboratory in Basovizza (Trieste, Italy) and the staff of the XAFS beamline are gratefully acknowledged for their support and technical assistance. We thank the Department of Chemistry of the

University of Genoa (Italy) for providing access to the HRTEM instrument.

Keywords: electrooxidation · ethanol · fuel cells · palladium · supported catalysts

[1] C. Lamy, A. Lima, V. LeRhun, F. Delime, C. Coutanceau, J.-M. Léger, *J. Power Sources* **2002**, *105*, 283–296.
[2] F. Vigier, S. Rousseau, C. Coutanceau, J.-M. Léger, C. Lamy, *Top. Catal.* **2006**, *40*, 111.
[3] E. Antolini, *J. Power Sources* **2007**, *170*, 1–12.
[4] J. S. Spendelow, A. Wieckowski, *Phys. Chem. Chem. Phys.* **2007**, *9*, 2654.
[5] K. Y. Chan, J. Ding, J. Ren, S. Cheng, K. Y. Tsang, *J. Mater. Chem.* **2004**, *14*, 505.
[6] H. Igarashi, T. Fujino, Y. Zhu, H. Uchida, M. Watanabe, *Phys. Chem. Chem. Phys.* **2001**, *3*, 306.
[7] C. R. K. Rao, D. C. Trivedi, *Coord. Chem. Rev.* **2005**, *249*, 613.
[8] R. Pattabiraman, *Appl. Catal. A: Gen.* **1997**, *153*, 9.
[9] H. T. Zheng, Y. Li, S. Chen, P. K. Shen, *J. Power Sources* **2006**, *163*, 371–375.
[10] P. K. Shen, C. Xu, *Electrochem. Commun.* **2006**, *8*, 184–188.
[11] C. Coutanceau, L. Demarconnay, C. Lamy, J.-M. Léger, *J. Power Sources* **2006**, *156*, 14–19.
[12] C. Xu, Z. Tian, P. Shen, S. P. Jiang, *Electrochim. Acta* **2008**, *53*, 2610–2618.
[13] C. Xu, P. K. Shen, Y. Liu, *J. Power Sources* **2007**, *164*, 527–531.
[14] M. Nie, H. Tang, Z. Wei, S. P. Jiang, P. K. Shen, *Electrochem. Commun.* **2007**, *9*, 2375–2379.
[15] C. Xu, L. Cheng, P. Shen, Y. Liu, *Electrochem. Commun.* **2007**, *9*, 997–1001.
[16] D. Yuan, C. Xu, Y. Liu, S. Tan, X. Wang, Z. Wei, P. K. Shen, *Electrochem. Commun.* **2007**, *9*, 2473–2478.
[17] F. P. Hu, Z. Wang, Y. Li, C. Li, X. Zhang, P. K. Shen, *J. Power Sources* **2008**, *177*, 61–66.
[18] Z. Wang, F. Hu, P. K. Shen, *Electrochem. Commun.* **2006**, *8*, 1764–1768.
[19] F. Hu, F. Ding, S. Song, P. K. Shen, *J. Power Sources* **2006**, *163*, 415–419.
[20] H. T. Zheng, Y. Li, S. Chen, P. K. Shen, *J. Power Sources* **2006**, *163*, 371–375.
[21] H. Wang, C. Xu, F. Cheng, S. Jiang, *Electrochem. Commun.* **2007**, *9*, 1212–1216.
[22] J. Zhang, M. Huang, H. Ma, F. Tian, W. Pan, S. Chen, *Electrochem. Commun.* **2007**, *9*, 1298–1304.
[23] G. Q. Lu, A. Crown, A. Wieckowski, *J. Phys. Chem. B* **1999**, *103*, 9700–9711.
[24] W.-r. Lee, M. G. Kim, J.-r. Choi, J.-L. Park, S. J. Ko, S. J. Oh, J. Cheon, *J. Am. Chem. Soc.* **2005**, *127*, 16090–16097.
[25] E. V. Spinacé, A. O. Neto, M. Linardi, *J. Power Sources* **2004**, *129*, 121–126.
[26] R. S. Jayashree, J. S. Spendelow, J. Yeom, C. Rastogi, M. A. Shannon, P. J. A. Kenis, *Electrochim. Acta* **2005**, *50*, 4674–4682.
[27] P. Waszczuk, T. M. Barnard, C. Rice, R. I. Masel, A. Wieckowski, *Electrochem. Commun.* **2002**, *4*, 599–603.
[28] A. Crown, C. Johnson, A. Wieckowski, *Surf. Sci.* **2002**, *506*, L268L274.
[29] S. R. Brankovic, J. X. Wang, R. R. Adzic, *Surf. Sci.* **2001**, *474*, L173L179.
[30] S. R. Brankovic, J. X. Wang, R. R. Adzic, *Electrochem. Solid-State Lett.* **2001**, *4*, A217.
[31] S. R. Brankovic, J. McBreen, R. R. Adzic, *J. Electroanal. Chem.* **2001**, *503*, 99–104.
[32] K. Sasaki, Y. Mo, J. X. Wang, M. Balasubramanian, F. Uribe, J. McBreen, R. R. Adzic, *Electrochim. Acta* **2003**, *48*, 3841–3849.
[33] Z. Shi, S. Wu, J. A. Szpunar, *Chem. Phys. Lett.* **2006**, *422*, 147.
[34] T. Nakashima, S. Nohara, H. Hiroshi, C. Iwakura, *Res. Chem. Intermed.* **2006**, *32*, 561.
[35] C. Bianchini, F. Vizza, unpublished results.
[36] K. Lohrberg, P. Kohl, *Electrochim. Acta* **1984**, *29*, 1557–1561.
[37] G. Sheela, M. Pushpavanam, S. Pushpavanam, *Int. J. Hydrogen Energy* **2002**, *27*, 627–633.
[38] J. Larminie, A. Dicks in *Fuel Cell Systems Explained*, Wiley, West Sussex **2003**, p. 135.
[39] S.-M. Park, N. C. Chen, N. Doddapaneni, *J. Electrochem. Soc.* **1995**, *142*, 40.
[40] A. Kowal, S. N. Port, R. J. Nichols, *Catal. Today* **1997**, *38*, 483–492.
[41] A. Kowal, C. Gutierrez, *J. Electroanal. Chem.* **1995**, *395*, 243–247.
[42] M. A. Abdel Rahim, R. M. A. Hameed, M. W. Khalil, *J. Power Sources* **2004**, *134*, 160–169.
[43] T. Kobayashi, J. Otomo, C.-j Wen, H. Takahashi, *J. Power Sources* **2003**, *124*, 34–39.
[44] F. Vitse, M. Cooper, G. Botte, *J. Power Sources* **2005**, *142*, 18–26.
[45] G. Botte, F. Vitse, M. Cooper, US 0211569A1, **2005**.
[46] E. Sommerfeld, DE 1254132, **1997**.
[47] K. Hata, *New Hydrogenation Catalysts*, Halsted, New York, **1971**.
[48] B. Veeraraghavan, H. Kim, B. Popov, *Electrochim. Acta* **2004**, *49*, 3143–3154.
[49] B. Veeraraghavan, B. Haran, S. P. Kumaraguru, B. Popov, *J. Electrochem. Soc.* **2003**, *150*, B131.
[50] C. Bock, C. Paquet, M. Couillard, G. A. Botton, B. R. MacDougall, *J. Am. Chem. Soc.* **2004**, *126*, 8028–8037.
[51] Z. Zhou, S. Wang, W. Zhou, G. Wang, L. Jiang, W. Li, S. Song, J. Liu, G. Sun, Q. Xin, *Chem. Commun.* **2003**, 394.
[52] C. Luo, Y. Zhang, Y. Wang, *J. Mol. Catal. A: Chem.* **2005**, *229*, 7–12.
[53] J. M. Basset, J. P. Candy, C. Copéret, F. Lefebvre, E. A. Quadrelli, *Nanotechnology in Catalysis, Vol. 2* (Eds.: B. Zhou, S. Hermans, G. Somorjai), Springer, Berlin, **2004**, p. 447.
[54] P. Barbaro, C. Bianchini, V. Dal Santo, A. Meli, S. Moneti, C. Pirovano, R. Psaro, L. Sordelli, F. Vizza, *Organometallics* **2008**, *27*, 2809–2824.
[55] XRD data were extracted from PDF-2 containing ICDD (International Centre for Diffraction Data) experimental powder data collection: http://www.icdd.com.
[56] M. R. Tarasevich, Z. R. Karichev, V. A. Bogdanovskaya, E. N. Lubnin, A. V. Kapustin, *Electrochem. Commun.* **2005**, *7*, 141–146.
[57] M. A. Abdel Rahim, R. M. A. Hameed, M. W. Khalil, *J. Power Sources* **2004**, *135*, 42–51.
[58] J. Bagchi, S. K. Bhattacharya, *J. Power Sources* **2007**, *163*, 661–670.
[59] Z. B. Wang, G. P. Yin, J. Zhang, Y. C. Sun, P. F. Shi, *Electrochim. Acta* **2006**, *51*, 5691–5697.
[60] S. Sen Gupta, J. Datta, *J. Power Sources* **2004**, *145*, 124–132.
[61] F.-g. Luo, Q.-j. Chen, Z.-l. Yin, *Trans. Nonferrous Met. Soc. China* **2007**, *17*, 654.
[62] S. Deabate, F. Fourgeot, F. Henn, *Electrochim. Acta* **2006**, *51*, 5430–5437.
[63] S. L. Medway, C. A. Lucas, A. Kowal, R. J. Nichols, D. Johnson, *J. Electroanal. Chem.* **2006**, *587*, 172–181.
[64] A. Roessler, D. Crettenand, O. Dossenbach, W. Marte, P. Rys, *Electrochim. Acta* **2002**, *47*, 1989–1995.
[65] A. Petrauskas, L. Grinceviciene, A. Èeðûnienë, R. Juðkënas, *Electrochim. Acta* **2005**, *50*, 1189–1196.
[66] R. Wang, W. Ye, C. Ma, C. Wang, *Mater. Charact.* **2008**, *59*, 108.
[67] M. Bouanani, F. Cherkaoui, R. Fratesi, R. Roventi, G. Barucca, *J. Appl. Electrochem.* **1999**, *29*, 637.
[68] C.-C. Hu, T.-C. Wen, *Electrochim. Acta* **1996**, *41*, 1505.
[69] C.-C. Hu, T.-C. Wen, *Electrochim. Acta* **1995**, *40*, 495.
[70] A. E. Bolzán, A. J. Arvia, *J. Electroanal. Chem.* **1992**, *157*, 247.
[71] V. M. Barragán, A. Heinzel, *J. Power Sources* **2002**, *104*, 66–72.
[72] K. Scott, E. Yu, G. Vlachogiannopoulos, M. Shivare, N. Duteanu, *J. Power Sources* **2008**, *175*, 452–457.
[73] J. Huang, Z. Liu, C. He, L. M. Gan, *J. Phys. Chem. B* **2005**, *109*, 16644–16649.

Received: September 26, 2008
Published online on December 29, 2008

